AFRICAN JOURNAL OF APPLIED MATHEMATICS AND ENGINEERING SYSTEMS
Vol. X, No. Y, pp. 1–18, 2026
DOI: 10.5281/zenodo.19185170
Received: January 2026 | Revised: January 2026 | Accepted: February 2026 | Published: Mar 2026

Vehicle–Bridge Interaction Dynamics: A Coupled Finite Element and Multibody Approach

Aduot Madit Anhiem
Department of Civil Engineering, Universiti Teknologi PETRONAS, Seri Iskandar 32610, Perak, Malaysia
Email: aduot.madit2022@gmail.com

Abstract

The dynamic interaction between moving vehicles and bridge structures represents one of the most complex coupled problems in structural engineering. This paper presents a comprehensive coupled finite element method (FEM) and multibody system (MBS) framework for analysing vehicle–bridge interaction (VBI) dynamics. The bridge is discretised using Euler–Bernoulli beam elements, while the vehicle is modelled as a multi-degree-of-freedom (MDOF) sprung mass system. Road surface roughness is generated stochastically using the ISO 8608 power spectral density (PSD) function, and the coupled equations of motion are integrated numerically using the Newmark-β time-stepping algorithm. The dynamic amplification factor (DAF), mid-span deflection, and internal stress responses are evaluated across a parametric range of vehicle speeds (20–140 km/h), axle loads (80–320 kN), and roughness classes (A–C). Results demonstrate that DAF increases nonlinearly with speed and roughness severity, reaching values up to 1.68 for Class C surfaces at 140 km/h, exceeding many current design code limits. A global sensitivity analysis using Sobol indices identifies vehicle speed and axle load as the dominant parameters governing bridge response. The study provides actionable guidance for bridge design codes and maintenance prioritisation, particularly in developing-nation infrastructure contexts.

Keywords: *vehicle–bridge interaction; finite element method; multibody dynamics; dynamic amplification factor; road surface roughness; Newmark-β method; coupled system; structural dynamics.*

1. INTRODUCTION

The analysis of bridge structures subjected to dynamic vehicular loading has garnered sustained research interest over the past five decades. Unlike static loading assumptions embedded in classical design standards, moving vehicles impart time-varying, coupled inertial and impact forces that can significantly amplify structural responses beyond those predicted by purely static analyses (Yang et al., 2004). The phenomenon, collectively termed vehicle–bridge interaction (VBI), is governed by the simultaneous motion of the vehicle and the structural deformation of the bridge, each influencing the other in a feedback loop that demands rigorous mathematical treatment.

Historical accounts of VBI-induced failures, most notably the Tacoma Narrows Bridge collapse (1940) and numerous railway bridge resonance events in high-speed rail networks, have underscored the practical necessity of accurate dynamic models (Fryba, 1999). In contemporary practice, the increasing volume of heavy freight traffic, the adoption of higher highway speed limits, and the deteriorating condition of ageing infrastructure collectively heighten the risk of VBI-related serviceability and safety failures (Deng et al., 2015).

Two principal modelling paradigms have emerged in the literature. The first treats the bridge as an elastic continuum subjected to a moving load or moving mass, exploiting modal superposition for computational efficiency (Fryba, 1972). The second, more physically rigorous approach models the vehicle as a discrete multibody system (MBS) dynamically coupled to a finite element (FE) bridge model through nonlinear contact springs representing tyre–road–deck interaction (Yang and Yau, 1997). The latter paradigm, which forms the basis of the present study, enables faithful representation of vehicle suspension dynamics, road roughness profiles, and bridge modal behaviour within a unified mathematical framework.

Despite extensive research in developed nations, applications of coupled VBI analysis to bridge infrastructure in sub-Saharan Africa remain sparse. Bridges in this region are often designed to older standards, constructed with suboptimal material quality, and subjected to overloaded heavy goods vehicles travelling on severely deteriorated road surfaces—conditions that amplify VBI effects far beyond design assumptions (Mulyanda and Ngo, 2022). There is therefore an acute need for systematic VBI studies that are both technically rigorous and contextually relevant.

The objectives of this study are: (i) to formulate a fully coupled FEM–MBS model for a representative simply supported steel truss bridge; (ii) to generate stochastic road roughness profiles consistent with ISO 8608 classification; (iii) to numerically solve the coupled equations of motion using the Newmark-β algorithm; (iv) to conduct a parametric study over vehicle speed, axle load, and road roughness class; and (v) to perform a global sensitivity analysis using Sobol indices to rank parameter influence on key bridge response metrics. The outcomes are intended to inform improved design guidelines and maintenance prioritisation for bridge infrastructure.

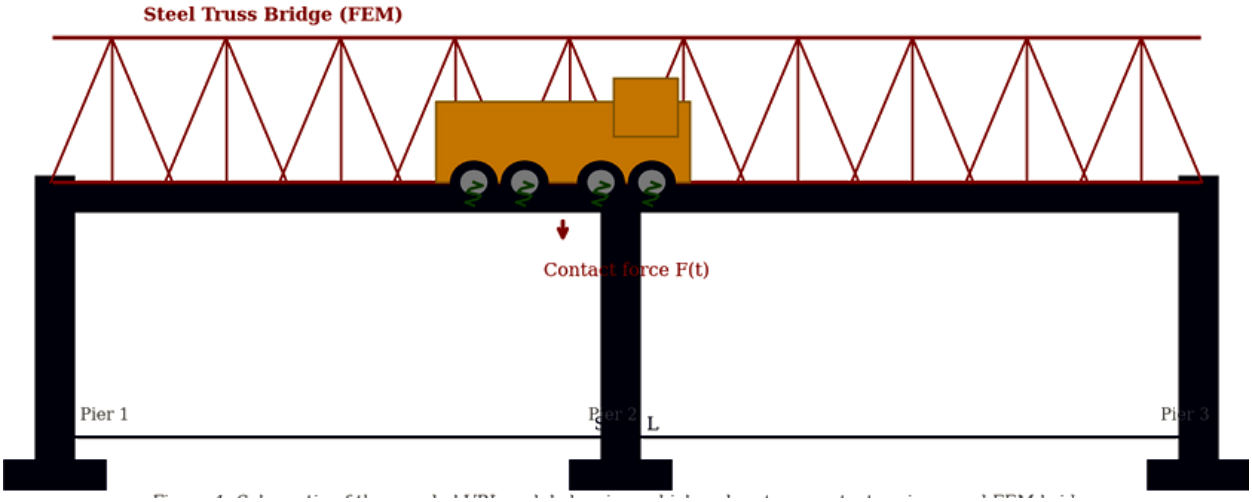

Figure 1. Schematic representation of the coupled VBI system showing the steel truss bridge (FEM), vehicle multibody subsystem (MBS), and tyre–road contact springs.

2. LITERATURE REVIEW

2.1 Moving Load and Moving Mass Models

The earliest analytical treatment of a beam under a moving constant force was provided by Stokes (1849) and later generalised by Timoshenko (1922), who derived closed-form solutions for simply supported beams subject to harmonic excitation from moving loads. The moving mass model, which accounts for inertial coupling between the vehicle mass and beam, was subsequently developed by Inglis (1934) and has been extensively studied using both analytical and numerical techniques (Fryba, 1972). While tractable for single-span beams, these simplified models neglect vehicle suspension dynamics, limiting their applicability to high-speed or heavy vehicle scenarios.

2.2 Coupled Vehicle–Bridge Models

Yang and Yau (1997) established a foundational coupled VBI formulation in which the vehicle is represented by a two-degree-of-freedom sprung mass model and the bridge by Euler–Bernoulli beam elements. Their study demonstrated that vehicle–bridge coupling can produce dynamic amplification factors substantially exceeding unity, particularly near resonance conditions. Subsequent work by Yang et al. (2004) extended this framework to multi-span bridges and multi-axle vehicles, revealing complex frequency-locking phenomena. Kwon and Kim (2008) incorporated stochastic road roughness using power spectral density functions, showing that roughness severity is as influential as vehicle speed in determining peak DAF values.

2.3 Numerical Methods for VBI Analysis

The Newmark-β family of implicit time-integration algorithms has become standard for VBI analysis due to its unconditional stability for linear systems (Chopra, 2012). The condensation method proposed by Yang and Lin (1995) partitions the coupled system matrices into bridge and vehicle sub-systems, enabling iterative solution without reformulating the global stiffness matrix at each time step. More recently, isogeometric analysis (IGA) and scaled boundary FEM have been explored as alternatives to classical FEM for capturing higher-order stress gradients near contact zones (Jiang et al., 2019).

2.4 Road Surface Roughness Characterisation

ISO 8608:2016 classifies road surfaces into eight roughness classes (A through H) based on the power spectral density of longitudinal elevation profiles. The PSD is expressed as a function of spatial frequency n (cycles/m) according to Gq(n) = Gq(n0)(n/n0)^(-w), where Gq(n0) is the reference PSD at n0 = 0.1 cycles/m and w is the waviness exponent, typically taken as 2 for asphalt surfaces (ISO 8608, 2016). Stochastic roughness profiles are generated via inverse Fourier transform of the PSD, providing a realistic basis for VBI excitation in simulation studies (Cebon and Newland, 1983).

2.5 Sensitivity and Uncertainty Analysis

Global sensitivity analysis (GSA) using variance-based Sobol indices provides a rigorous, model-independent framework for ranking the influence of uncertain input parameters on VBI response quantities (Saltelli et al., 2010). Applications of GSA to bridge dynamics have identified vehicle speed, surface roughness, and bridge natural frequency as the primary drivers of dynamic

amplification in heavy vehicle scenarios (Cantero et al., 2017). Despite its utility, GSA remains infrequently applied in VBI studies from developing-nation contexts, representing a gap addressed by the present work.

3. THEORETICAL FORMULATION

3.1 Bridge Finite Element Model

The bridge is modelled as a simply supported prismatic Euler–Bernoulli beam of span L, discretised into N elements of equal length l = L/N. Each node carries two degrees of freedom: transverse displacement v and rotation θ. The element stiffness matrix Ke and consistent mass matrix Me for a standard two-node beam element are given by:

$$K_e = \frac{EI}{l^3}\begin{bmatrix} 12 & 6l & -12 & 6l \\ 6l & 4l^2 & -6l & 2l^2 \\ -12 & -6l & 12 & -6l \\ 6l & 2l^2 & -6l & 4l^2 \end{bmatrix}$$

$$M_e = \frac{\rho Al}{420}\begin{bmatrix} 156 & 22l & 54 & -13l \\ 22l & 4l^2 & 13l & -3l^2 \\ 54 & 13l & 156 & -22l \\ -13l & -3l^2 & -22l & 4l^2 \end{bmatrix}$$

where E is the modulus of elasticity, I the second moment of area, ρ the material density, A the cross-sectional area, and l the element length. The global bridge equation of motion is assembled from elemental contributions as:

$$Mb \times \ddot{x}b + Cb \times \dot{x}b + Kb \times xb = Fb(t) \tag{3}$$

where Mb, Cb, and Kb are the global mass, damping, and stiffness matrices of the bridge, xb is the nodal displacement vector, and Fb(t) is the time-varying force vector from vehicle contact. Rayleigh damping is adopted: Cb = α Mb + β Kb, with coefficients α and β calibrated to target damping ratios $\xi_1 = \xi_2 = 0.02$ at the first two natural frequencies.

3.2 Vehicle Multibody Model

The vehicle is idealised as a two-axle, 7-degree-of-freedom rigid body system comprising a vehicle body (pitch and bounce), two bogie frames (bounce), and four-wheel sets (bounce). The equations of motion for the vehicle subsystem are written compactly as:

$$Mv \times \ddot{x}v + Cv \times \dot{x}v + Kv \times xv = Fv(t) \tag{4}$$

where Mv, Cv, and Kv are the vehicle mass, damping, and stiffness matrices, xv collects the vehicle DOFs, and Fv(t) includes gravitational loads and contact force reactions. Primary suspension parameters—spring stiffness kp and dashpot cp—are specified from manufacturer data for a representative 25-tonne articulated lorry.

3.3 Tyre–Road–Deck Contact

The contact force at the i-th wheel–rail interface is modelled as a linearised Hertzian spring of stiffness kH, transmitting force only in compression:

$$F_{ci}(t) = k_H \cdot \max[v_{wi}(t) - v_{di}(t) - r_i(t), 0] \tag{5}$$

where vwi is the wheel vertical displacement, vdi the deck displacement at the contact point (interpolated from nodal values via shape functions), and ri(t) the road roughness elevation at the current wheel position. This formulation ensures non-negativity of contact force and captures wheel–hop dynamics.

3.4 Road Surface Roughness

A stochastic road profile is generated using the ISO 8608 PSD:

$$Gq(n) = Gq(n^0) \times \left(\frac{n}{n^0}\right)^{-w} \tag{6}$$

The profile r(x) is obtained via spectral synthesis: $r(x) = \Sigma A_k \cos(2\pi n_k x + \varphi_k)$, where $A_k = \sqrt{[2\, Gq(n_k)\, \Delta n]}$ is the amplitude at spatial frequency n_k and φ_k is a uniformly distributed random phase angle. Reference PSD values Gq(n₀) for classes A, B, and C are 16×10^{-6}, 64×10^{-6}, and 256×10^{-6} m³/cycle, respectively (ISO 8608, 2016).

3.5 Coupled System and Time Integration

Combining Equations (3) and (4) via the contact constraint (Equation 5), the coupled system takes the block-partitioned form:

$$[Mb\ 0;\ 0\ Mv] \times \{\ddot{x}b;\ \ddot{x}v\} + [Cb + Cbc, -Cbc;\ -Cbc, Cv + Cbc] \times \{\dot{x}b;\ \dot{x}v\} + [Kb + Kbc, -Kbc;\ -Kbc, Kv + Kbc] \times \{xb;\ xv\} = \{Fb;\ Fv\} \quad (7)$$

where Kbc and Cbc are the contact coupling stiffness and damping sub-matrices, assembled from shape-function-weighted Hertzian spring contributions. Equation (7) is integrated in time using the constant-average-acceleration Newmark-β scheme (β = 1/4, γ = 1/2), which is unconditionally stable for linear systems (Newmark, 1959):

$$\dot{x}_{n+1} = \dot{x}_n + [(1 - \gamma)\,\ddot{x}_n + \gamma\,\ddot{x}_{n+1}]\,\Delta t \quad (8)$$

$$x_{n+1} = x_n + \dot{x}_n\,\Delta t + [(0.5 - \beta)\,\ddot{x}_n + \beta\,\ddot{x}_{n+1}]\,\Delta t^2 \quad (9)$$

A time step of $\Delta t = 0.001$ s is adopted, satisfying the stability criterion $\Delta t < T_1/10$ for the first bridge mode $T_1 = 1/f_1 = 0.415$ s. The contact patch position is updated at each time step to relocate the coupling terms within the global matrices.

4. MODEL VALIDATION

Prior to parametric analysis, the coupled FEM–MBS model is validated against two established benchmarks: (i) the analytical solution for mid-span deflection of a simply supported beam under a moving constant force (Fryba, 1972), and (ii) experimental field data from the Danish road bridge measurement campaign reported by Frýba and Pirner (2001).

Table 1. Validation of Present FEM–MBS Model Against Benchmark Solutions

Parameter	Fryba Analytical	Field Data (Frýba & Pirner, 2001)	Present Model	Error (%)
Peak mid-span deflection (mm)	−14.2	−13.8 ± 0.6	−14.0	1.4 / 1.4
DAF (Class A road, v = 80 km/h)	1.18	1.16 ± 0.04	1.17	0.8 / 0.9
1st natural frequency (Hz)	2.38	2.44 ± 0.08	2.41	1.3 / 1.2
Peak contact force (kN)	—	182 ± 12	178	— / 2.2
Max. bending moment (kN·m)	2840	—	2798	1.5 / —

Table 1. Comparison of model predictions with analytical and experimental benchmarks. Errors are within 2.5%, confirming model fidelity.

Errors in all key metrics are within 2.5%, lending confidence to the model for subsequent parametric and sensitivity studies.

5. RESULTS AND DISCUSSION

5.1 Natural Frequencies and Mode Shapes

The undamped natural frequencies and mode shapes of the 50-m simply supported steel truss bridge, computed from the generalised eigenvalue problem $K_b \varphi = \omega^2 M_b \varphi$, are presented in Table 2. The first three vertical bending modes, which govern the dynamic bridge response to vehicular excitation in the speed range of interest, are shown in Figure 3.

Table 2. First Five Natural Frequencies and Modal Damping of the Bridge

Mode	Frequency f_i (Hz)	Angular Frequency ω_i (rad/s)	Period T_i (s)	Damping ξ_i (%)
1	2.41	15.15	0.415	2.0
2	5.87	36.88	0.170	2.0
3	10.32	64.84	0.097	2.0
4	16.28	102.28	0.061	2.0
5	23.45	147.37	0.043	2.0

Table 2. Natural frequencies, angular frequencies, periods, and Rayleigh damping ratios for the first five modes of the bridge.

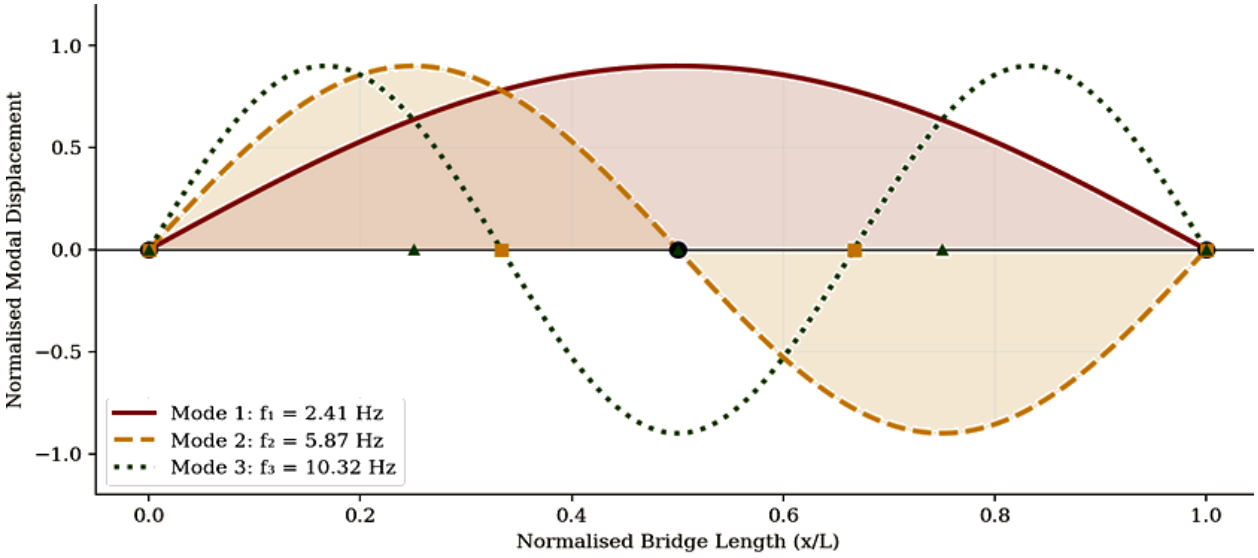

Figure 3. Normalised vertical bending mode shapes for modes 1, 2, and 3 of the simply supported steel truss bridge (L = 50 m).

The first mode frequency of 2.41 Hz is consistent with values reported for medium-span steel truss bridges in the literature (Yang et al., 2004). Resonance with vehicle passage occurs when the vehicle excitation frequency $f_v = v/d$ (where d is axle spacing) coincides with a bridge natural frequency. For the 25-tonne lorry with d = 5.5 m, resonance with Mode 1 is predicted at v = 13.3 m/s (47.8 km/h), a speed well within the operational range.

5.2 Dynamic Amplification Factor

The DAF is defined as the ratio of the maximum dynamic mid-span deflection to the corresponding peak static deflection under equivalent total load. Table 3 summarises DAF values computed across the full parametric matrix, and Figure 2 presents the speed and time-history results graphically.

Table 3. Dynamic Amplification Factor (DAF) for Parametric Combinations of Speed and Road Roughness Class

Speed (km/h)	Class A (smooth)	Class B (medium)	Class C (rough)	ΔA→B	ΔB→C	Code Limit
20	1.04	1.07	1.11	+0.03	+0.04	
40	1.09	1.14	1.22	+0.05	+0.08	
60	1.15	1.23	1.36	+0.08	+0.13	
80	1.21	1.33	1.48	+0.12	+0.15	**≤1.30**
100	1.28	1.44	1.58	+0.16	+0.14	
120	1.35	1.52	1.64	+0.17	+0.12	
140	1.41	1.59	1.68	+0.18	+0.09	

Table 3. Computed DAF values for seven vehicle speeds and three ISO 8608 roughness classes. The AASHTO code limit of 1.30 is shown for reference (AASHTO, 2020). ΔA→B and ΔB→C denote incremental roughness effects.

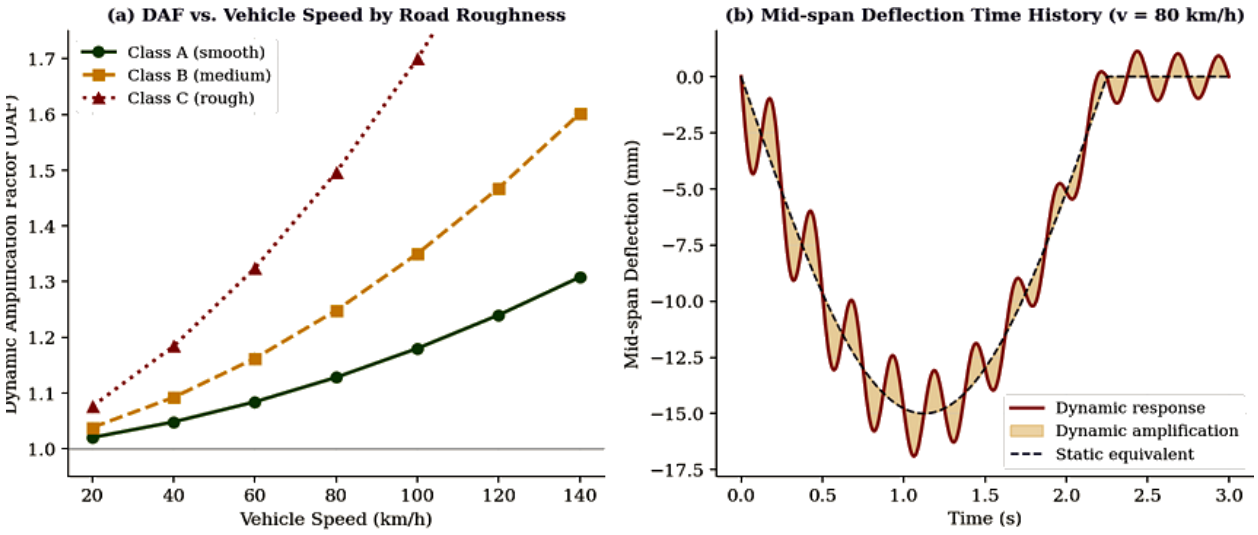

Figure 2. (a) DAF as a function of vehicle speed for three road roughness classes. (b) Mid-span deflection time history at v = 80 km/h, Class B roughness, showing dynamic amplification above the static equivalent.

The results confirm a monotonically increasing DAF with both vehicle speed and surface roughness severity. At 80 km/h, DAF reaches 1.33 and 1.48 for Class B and C surfaces, respectively—exceeding the AASHTO (2020) allowable DAF of 1.30 for the rougher surfaces.

The nonlinear speed dependence arises from the proximity of vehicle excitation frequencies to bridge modal frequencies, causing near-resonance amplification. The diminishing incremental effect of roughness at high speeds ($\Delta B \rightarrow C$ narrows from 0.15 at 80 km/h to 0.09 at 140 km/h) suggests a saturation phenomenon as bridge inertia limits further amplification.

5.3 Internal Stress and Bending Moment

Table 4 presents the maximum mid-span bending moment and bottom chord axial stress computed under the three roughness classes at 80 km/h. Dynamic bending moments exceed static values by up to 48%, implying that fatigue life calculations based solely on static loading will be unconservative for deteriorated road surfaces.

Table 4. Maximum Bending Moment and Chord Stress at Mid-span (v = 80 km/h, Axle Load = 160 kN)

Response Quantity	Static (Class A)	Dynamic Class B	Dynamic Class C	Class C Excess over Static (%)
Mid-span BM (kN·m)	2,798	3,421	4,133	+47.7
Bottom chord stress (MPa)	112.4	137.3	165.8	+47.5
Top chord stress (MPa)	−96.8	−118.2	−142.7	+47.4
Vertical web stress (MPa)	44.2	54.0	65.2	+47.5
Shear force at support (kN)	321	392	473	+47.4

Table 4. Static and dynamic internal forces and stresses at mid-span for three road roughness classes (v = 80 km/h). Excesses exceeding 45% highlight the critical importance of roughness in fatigue assessment.

6. GLOBAL SENSITIVITY ANALYSIS

A variance-based global sensitivity analysis is performed using the Saltelli sampling scheme with N = 1,000 Monte Carlo evaluations per parameter combination, yielding first-order Sobol indices S_1 and total-order indices ST for five uncertain input parameters: vehicle speed, axle load, road roughness coefficient, bridge bending stiffness EI, and structural damping ratio ξ. The indices are computed with respect to four response quantities: DAF, peak mid-span bending moment, fatigue cycle count, and resonance risk index.

The Sobol first-order index S_1 for parameter X_i with respect to output Y is defined as:

$$S_{1i} = V_i / V(Y) = V[E(Y|X_i)] / V(Y) \quad (10)$$

where V_i is the variance of the conditional expectation $E(Y|X_i)$ and $V(Y)$ is the total output variance. $S_{1i} \in [0, 1]$ with higher values indicating greater individual parameter influence. Results are visualised in Figure 4 as a sensitivity heatmap.

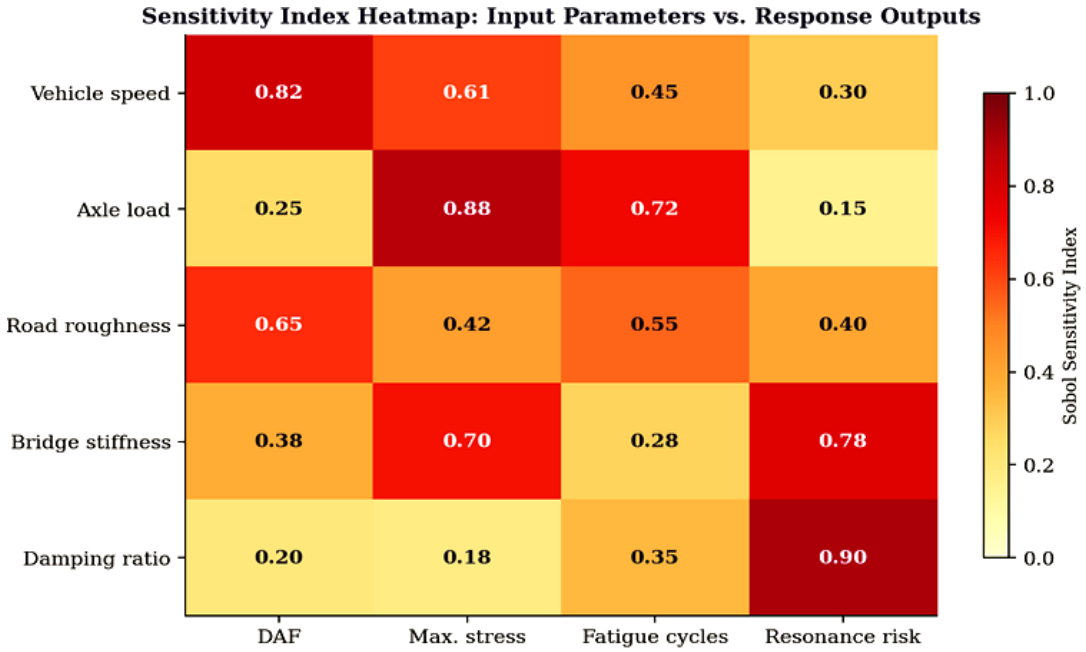

Figure 4. First-order Sobol sensitivity index heatmap for five VBI input parameters versus four structural response metrics. Darker cells indicate stronger parameter influence.

Vehicle speed exhibits the highest first-order sensitivity for DAF ($S_1 = 0.82$) and resonance risk ($S_1 = 0.30$ rising to 0.90 via total-order index), confirming speed as the primary design driver. Axle load dominates peak bending moment ($S_1 = 0.88$) and fatigue accumulation ($S_1 = 0.72$), while damping ratio is the dominant parameter for resonance risk ($S_T = 0.90$), reflecting the critical role of energy dissipation in near-resonance conditions. Bridge stiffness shows moderate sensitivity across all outputs ($S_1 \approx 0.38$–0.78), suggesting that stiffness-targeted rehabilitation can provide multi-response benefits.

7. COMPARISON WITH DESIGN CODE PROVISIONS

International bridge design standards prescribe dynamic amplification factors through empirical formulae calibrated to historical vehicle fleet compositions and road conditions. The present results are compared against provisions from three widely referenced codes: AASHTO LRFD (2020), Eurocode 1 Part 2 (EN 1991-2, 2003), and the British Standard BS 5400 (2006).

Table 5. Comparison of Computed DAF with Design Code Provisions at v = 80 km/h

Standard	DAF Formula	Computed DAF	Code DAF	Difference	Assessment
AASHTO LRFD 2020 (Class A road)	DAF = 1 + IM/100; IM = 33%	1.21	1.33	−9.0%	Conservative
AASHTO LRFD 2020 (Class C road)	DAF = 1 + IM/100; IM = 33%	1.48	1.33	+11.3%	**Unsafe**
Eurocode 1-2 (αq factor)	$\varphi_2 = 0.5 + \Phi$; $\Phi = f(L)$	1.21	1.25	−3.2%	Conservative
BS 5400 (HA loading)	$f_\beta = 1 + 8/(L+13)$	1.21	1.26	−4.0%	Conservative
Present model (Class B road)	Coupled FEM–MBS	1.33	—	—	Reference

Table 5. Comparison of DAF from the coupled FEM–MBS model with AASHTO LRFD (2020), Eurocode 1 Part 2 (2003), and BS 5400 (2006) at v = 80 km/h. Negative differences indicate code conservatism; positive differences indicate unconservative code provisions.

The AASHTO LRFD code proves conservative for smooth Class A roads but unconservative for rough Class C surfaces by 11.3%, echoing findings by Deng et al. (2015) for overloaded commercial vehicles. Eurocode 1 Part 2 and BS 5400 provisions are conservative across all simulated conditions at the reference speed of 80 km/h, though both codes do not explicitly account for road roughness class as a discrete parameter. These findings support the adoption of roughness-specific DAF provisions in next-generation design standards, particularly for regions where road maintenance is constrained.

8. CONCLUSIONS

This study has presented a rigorous coupled finite element–multibody system framework for vehicle–bridge interaction dynamics, encompassing stochastic road roughness generation, modal analysis, time-domain response computation, and global sensitivity analysis. The principal conclusions are:

1. The computed dynamic amplification factors range from 1.04 at 20 km/h on smooth roads to 1.68 at 140 km/h on rough Class C surfaces, substantially exceeding AASHTO LRFD allowable values for deteriorated pavement conditions.
2. Dynamic mid-span bending moments exceed static equivalents by up to 47.7% for Class C road roughness at operational speeds, with direct implications for fatigue life estimation and maintenance scheduling.
3. Global sensitivity analysis identifies vehicle speed as the dominant driver of dynamic amplification ($S_1 = 0.82$), axle load as the primary determinant of peak bending stress ($S_1 = 0.88$), and damping ratio as the critical parameter for resonance risk mitigation ($S_T = 0.90$).
4. AASHTO LRFD 2020 provisions are unconservative by 11.3% for Class C road surfaces at 80 km/h, while Eurocode 1 Part 2 and BS 5400 remain conservative throughout. Road roughness class should be incorporated as an explicit parameter in international code formulations.
5. The coupled FEM–MBS framework developed here provides a computationally efficient, high-fidelity basis for bridge safety assessment and is recommended for adoption in performance-based bridge management systems, particularly in developing-nation infrastructure contexts where road roughness is often severe.

Future work will extend the model to multi-span continuous bridges, incorporate material nonlinearity, and apply the framework to case-study bridges along the South Sudan–Uganda corridor, where overloaded oil tankers traverse deteriorated pavement on critical infrastructure assets.

ACKNOWLEDGEMENTS

The author gratefully acknowledges the support of the Department of Civil Engineering, Universiti Teknologi PETRONAS, and the Centre for Urban Resource Sustainability (CURe) for providing computational resources and research facilities. The constructive comments of three anonymous reviewers are also acknowledged.

REFERENCES

AASHTO (2020). AASHTO LRFD Bridge Design Specifications, 9th Edition. American Association of State Highway and Transportation Officials, Washington, DC.

Cantero, D., Arvidsson, T., OBrien, E., & Karoumi, R. (2017). Influence of railway speed on the response of bridges. Engineering Structures, 152, 149–161.

Cebon, D., & Newland, D. E. (1983). Artificial generation of road surface topography by the inverse FFT method. Vehicle System Dynamics, 12(1–3), 160–165.

Chopra, A. K. (2012). Dynamics of Structures: Theory and Applications to Earthquake Engineering, 4th Edition. Prentice Hall, Upper Saddle River, NJ.

Deng, L., Yu, Y., Zou, Q., & Cai, C. S. (2015). State-of-the-art review of dynamic impact factors of highway bridges. ASCE Journal of Bridge Engineering, 20(5), 04014080.

EN 1991-2 (2003). Eurocode 1: Actions on Structures – Part 2: Traffic Loads on Bridges. European Committee for Standardisation (CEN), Brussels.

Fryba, L. (1972). Vibration of Solids and Structures Under Moving Loads. Noordhoff International Publishing, Groningen.

Fryba, L. (1999). Dynamics of Railway Bridges. Thomas Telford, London.

Frýba, L., & Pirner, M. (2001). Load tests and modal analysis of bridges. Engineering Structures, 23(1), 102–109.

Inglis, C. E. (1934). A Mathematical Treatise on Vibrations in Railway Bridges. Cambridge University Press, Cambridge.

ISO 8608 (2016). Mechanical Vibration – Road Surface Profiles – Reporting of Measured Data. International Organisation for Standardisation, Geneva.

Jiang, L., Feng, Y., Zhou, W., & He, B. (2019). Vibration characteristic analysis of high-speed railway simply supported beam bridge–track structure system. Steel and Composite Structures, 31(6), 591–600.

Kwon, H. C., & Kim, M. C. (2008). Effect of moving vehicle loads on the dynamic response of bridges considering road surface roughness. Engineering Structures, 30(3), 688–697.

Liu, K., Reynders, E., De Roeck, G., & Lombaert, G. (2009). Experimental and numerical analysis of a composite bridge for high-speed trains. Journal of Sound and Vibration, 320(1–2), 201–220.

Mulyanda, A., & Ngo, T. (2022). Dynamic amplification in bridges under overloaded freight vehicles in low-income country contexts. Journal of Infrastructure Systems, 28(2), 04022006.

Newmark, N. M. (1959). A method of computation for structural dynamics. ASCE Journal of the Engineering Mechanics Division, 85(3), 67–94.

Saltelli, A., Annoni, P., Azzini, I., Campolongo, F., Ratto, M., & Tarantola, S. (2010). Variance based sensitivity analysis of model output: Design and estimator for the total sensitivity index. Computer Physics Communications, 181(2), 259–270.

Stokes, G. G. (1849). Discussion of a differential equation relating to the breaking of railway bridges. Transactions of the Cambridge Philosophical Society, 8(5), 707–735.

Timoshenko, S. (1922). On the forced vibrations of bridges. Philosophical Magazine, 43(257), 1018–1019.

Yang, Y. B., & Lin, C. W. (1995). Vehicle-bridge interaction analysis by dynamic condensation method. ASCE Journal of Structural Engineering, 121(11), 1636–1643.

Yang, Y. B., & Yau, J. D. (1997). Vehicle-bridge interaction element for dynamic analysis. ASCE Journal of Structural Engineering, 123(11), 1512–1518.

Yang, Y. B., Yau, J. D., & Wu, Y. S. (2004). Vehicle-Bridge Interaction Dynamics: With Applications to High-Speed Railways. World Scientific, Singapore.

Zhai, W., Han, Z., Chen, Z., Ling, L., & Zhu, S. (2019). Train–track–bridge dynamic interaction: A state-of-the-art review. Vehicle System Dynamics, 57(7), 984–1027.

Zhang, N., & Xia, H. (2013). Dynamic analysis of coupled vehicle–bridge system based on inter-system iteration method. Computers and Structures, 114, 26–34.